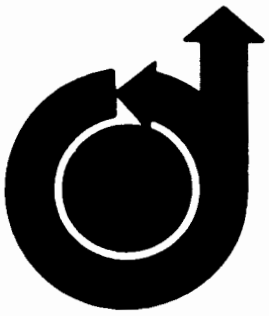

AIAA Paper No. 74-528

A THEORY TO PREDICT THE INCEPTION OF ROTATING STALL IN AXIAL FLOW COMPRESSORS

by
JOSEPH P. NENNI and GARY R. LUDWIG
Calspan Corporation
Buffalo, New York

AIAA 7th Fluid and Plasma Dynamics Conference

PALO ALTO, CALIFORNIA / JUNE 17-19, 1974

A THEORY TO PREDICT THE INCEPTION OF ROTATING STALL IN AXIAL FLOW COMPRESSORS*

Joseph P. Nenni** and Gary R. Ludwig†
Aerodynamic Research Department
Calspan Corporation,
Buffalo, New York

AIAA-33125

Abstract

A small disturbance stability theory has been developed to predict the inception of rotating stall in axial flow compressors. A two blade row and a single blade row version of the theory was developed. The theory indicates that the unsteady vorticity shed into the blade wakes by the variation in loss along the cascade axis is the mechanism controlling the stability of a given flow configuration. In this context, the slope of the curve of blade row loss versus inlet swirl is the most important blade row aerodynamic property controlling the stability of the flow. The two blade row theory indicates that axial blade row spacing controls the number of stall cells that form at inception. The neutral stability boundaries predicted by the theory correlate well with experimentally determined boundaries for inception of rotating stall.

Symbols

a	flow deflection parameter in single blade row theory, $\left(\frac{\partial \beta_2}{\partial \beta_1}\right)$
A_i, B_i, D_i	constants of integration in fundamental disturbance velocity solutions
c	complex exponent of disturbance velocity solutions
c_I, c_R	imaginary and real part of c, respectively
d	blade chord
H_i	total pressure in flow region i
j	$\sqrt{-1}$
n	number of stall cells
p	static pressure
p_i	perturbation pressure in flow region i
$\tilde{p}_i$	perturbation pressure function
q	$\frac{dn}{r}$ sec δ
r	mean blade-row radius
S_i	absolute swirl in flow region i, $(\tan \bar{\beta}_i)$
β_i	relative swirl in flow region i relative to blade row
t	time in laboratory fixed coordinate system
t_o	time in blade fixed coordinate system
u_i	x component of perturbation velocity in flow region i
U_i	x component of mean velocity in flow region i
$\hat{U}_i$	x component of total velocity in flow region i
U_{o_i}	x component of mean velocity relative to blade row
V_p	propagation velocity of disturbance or of rotating stall
w_i	y component of disturbance velocity in flow region i
W_i	y component of mean velocity in flow region i
x, y, z	cartesian coordinates in laboratory fixed coordinate system
x_o, y_o, z_o	cartesian coordinates in blade fixed coordinate system
X	total pressure loss coefficient
X'	$\partial X / \partial \beta$
$\bar{\beta}_i$	mean steady absolute flow angle in flow region i
$\hat{\beta}_i$	total absolute swirl angle in flow region i
Γ	circulation
δ	stagger angle
δ_{RM}	rotor stagger angle at mid-annulus
δ_{SM}	stator stagger angle at mid-annulus
η	z component of vorticity
λ	velocity solution, $(c + \bar{\Omega})$
ρ	density
ϕ_i	velocity function in flow region i
ψ_i	stream function in flow region i
$\bar{\Omega}$	normalized blade velocity
ω	vorticity vector

Introduction

The flow phenomenon known as rotating stall was first encountered in axial flow compressors during the mid-1940's. It was observed that there were large zones where the flow was separated from the compressor blade rows. These separated zones propagated relative to the blade row. The propagating or rotating feature gave the phenomenon its name. In many instances of engine failure, rotating stall has been identified as a precursor to destructive unsteady flows (e.g. surge) in an engine. Moreover, blade fatigue considerations will not allow a compressor to operate for prolonged periods in a large amplitude rotating stall mode. It is then desirable to develop a theory to predict inception conditions and identify the fundamental mechanisms involved so that design principles may be established to minimize the occurrence of rotating stall.

Rotating stall has, traditionally, been explained in terms of a flow blockage analog whereby the induced flow angularity from the blockage alleviates the stalling of blades on one side of the stall zone and promotes the stalling of blades on the opposite side of the stall zone. This simple explanation, while quite plausible, has not led to satisfactory progress in predicting theoretically the flow conditions which lead to the inception of rotating stall.

The first theories of rotating stall were given by Sears[1], Marble[2], Stenning et al[3], and Emmons et al[4]. The emphasis in these early works was on the prediction of propagation speed and number of stall cells whereas the emphasis in the present work is on prediction of inception conditions. Various blade row properties were assumed in these early studies and the salient features of these works are discussed and summarized

*This work was supported by the Air Force Aero Propulsion Laboratory, Turbine Engine Division, Components Branch under Contract No. F33615-70-C-1122.
**Research Engineer, Aerodynamic Research Department. Member AIAA.
† Principal Research Engineer, Aerodynamic Research Department. Member AIAA.

at length in Refs. 5 and 6. The details, therefore, will not be recounted here except to mention that the concept of a boundary layer lag time was considered important[1),(3),(5)]. Generally, good correlation with experiment was obtained only in those analyses in which the boundary layer lag time (or equivalently phase angle) was left free for adjustment. Moreover, when several sets of data were analyzed in the same fashion, no general conclusion could be drawn about the required phase lags[(5)].

The present analysis may be considered as an extension of the channel flow theory of Ref. 1. The fundamental extensions include the effects of finite chord length, allowance for flow turning through the blade row and more realistic representation of the loss characteristics of the blade row. In addition, the theory is also applied to a two blade row configuration. Some of the essential ideas and features of the present analysis were given by Whitehead[(7)] and Rannie and Marble[(8)]. These contributions were, however, not widely recognized because the theory was not fully exploited and comparisons between theory and experiment were very limited. Some of the important features of the present work are also included in the linearized theory given by Takata and Nagano[(9)]. However, Takata and Nagano emphasize the role of the nonlinear aspects in determining the propagation velocity and do not identify the fundamental mechanisms that produce rotating stall. In addition, they do not give direct comparisons on inception conditions.

The present theory is a small disturbance stability theory in that time dependent small disturbances are superimposed on the steady mean flow through a blade row, and the growth of the disturbances with time is determined for various flow configurations. The flow is considered stable if the disturbances die out or are damped with time, unstable if the disturbances grow or are amplified in time, and neutrally stable if the disturbance amplitude is not changing with time. The stall inception is assumed to correspond to the neutral stability boundary. The theory has been developed for an isolated blade row and a two blade row configuration. The isolated or single blade row analysis is principally described in this paper since this model allows the development of more explicit results and produces numerical results which are close to the two blade row case. The details of the two blade row development are presented in Ref. 10 and only the results will be summarized here.

The present analysis is a natural extension of the methods of formulation developed in Refs. 11 and 12. It was concluded in Ref. 12 that blade row losses would have to be included in the flow model in order to produce an instability. They have been included in the present flow model and the resulting correlation of theory and experiment validates the conclusion of Ref. 12.

The present theory, as have been all the previous rotating stall theories is an incomplete theory in that blade row performance data must be used as input to the theory. At present, it appears that the only satisfactory source of these data is experiment.

The flow model presently used is an incompressible two-dimensional finite-thickness actuator sheet model and is described in detail in the following sections. It is assumed that for high hub-to-tip ratios and low subsonic relative blade velocities the flow through a compressor blade row may be approximated by the flow through a two-dimensional cascade.

The effects of two variations in the flow model have also been considered. The inclusion of a time lag in the actuator (blade row) characteristics was considered along with an alternate boundary condition on the downstream pressure perturbation.

Single Blade Row Theory

The flow through an isolated blade row in incompressible flow is considered. A finite-thickness two-dimensional actuator-sheet was used to model the blade row and is shown in Fig. 1. (The subscript o's indicate quantities in a blade fixed coordinate system). The transformation between blade fixed coordinates and the laboratory fixed system is given by

$$x_o = x \,, \quad y_o = y - W_b t \,, \quad t_o = t$$

where W_b is the blade velocity in the laboratory fixed system. The conditions upstream of the blade row are denoted by a subscript 1 while conditions downstream of the blade row are denoted with a subscript 2. The mean flows upstream and downstream of the blade row are uniform but of different swirl angles. The finite thickness of the actuator retains the effects of the inertia of the fluid within the blade row and leads to propagation velocities which are weakly dependent upon blade chord. The mean absolute swirl angle in each region is denoted as $\bar{\beta}_i$ and the tangent of $\bar{\beta}_i$ is defined as S_i, the absolute swirl. For incompressible flow, U_i, the mean axial flow in each flow region i is a constant denoted as U_o and the nondimensional blade blade velocity is given by $\bar{\Omega} = W_b/U_o$. The relative swirl with respect to the blade row is given by $\mathcal{S}_i = S_i - \bar{\Omega}$.

Basically, the method of analysis is to determine the general solutions for disturbance velocities upstream and downstream of the actuator. These general solutions contain three unknown constants that must be determined by the boundary conditions. The boundary conditions are imposed by requiring matching conditions between upstream and downstream disturbance velocity solutions at the actuator. These matching conditions embody the assumed blade row aerodynamic characteristics.

All of the total flow quantities, which are denoted by a hat, are decomposed into steady and unsteady parts as

$$\hat{W}_i = W_i + w_i(t)$$

$$\hat{U}_i = U_i + u_i(t)$$

$$\hat{\beta}_i = \bar{\beta}_i + \beta_i'(t)$$

where the i designates the flow region. The unsteady parts are considered to be much smaller than the steady parts such that the equations of motion may be linearized in each flow region. The linearization process is exactly the same as that used in Ref. 11 and a solution for the disturbance

function of the form $\psi_i = \phi_i(x)\, e^{j(ct + ny/r)}$ is sought such that $u_i = \frac{\partial \psi_i}{\partial y}$ and $\omega_i = -\frac{\partial \psi_i}{\partial x}$. Here c is complex i.e., $(c = c_R + j c_I)$ and n is the number of stall cells. The resulting disturbance is spatially periodic in the y direction with period $\frac{2\pi r}{n}$ where r is the mean radius of the blade row. Neutral stability occurs when $c_I = 0$, instability when $c_I < 0$ and stability when $c_I > 0$. The appropriate ϕ_i are readily determined from the linearized Euler equations as

$$\phi_i(x) = A_i e^{-\frac{nx}{r}} + B_i e^{\frac{nx}{r}} + D_i e^{-j\frac{nx}{r}\left(\frac{cr}{nU_o} + S_i\right)} \qquad (1)$$

where the A_i, B_i, and D_i are constants to be determined by the boundary conditions.

To keep the flow quantities bounded at infinity upstream and downstream, we must have

$$A_1 = B_2 = 0$$

Further, requiring that the flow be irrotational at upstream infinity implies that $D_1 = 0$ since the A_i and B_i terms are irrotational.

These considerations reduce the number of undetermined constants to three and the disturbance velocities may then be expressed as

$$u_1 = B_1\, j\frac{n}{r}\, \exp\left[j\left(ct + \frac{ny}{r}\right) + \frac{nx}{r}\right] \qquad (2a)$$

$$\omega_1 = -B_1 \frac{n}{r} \exp\left[j\left(ct + \frac{ny}{r}\right) + \frac{nx}{r}\right] \qquad (2b)$$

$$u_2 = j\frac{n}{r}\left\{A_2 \exp\left[j\left(ct + \frac{ny}{r}\right) - \frac{nx}{r}\right] + D_2 \exp\left[j\left(ct + \frac{ny}{r}\right) - j\frac{nx}{r}\left(\frac{cr}{nU_o} + S_2\right)\right]\right\} \qquad (2c)$$

$$\omega_2 = \frac{n}{r} A_2 \exp\left[j\left(ct + \frac{ny}{r}\right) - \frac{nx}{r}\right] + j\frac{n}{r}\left(\frac{cr}{nU_o} + S_2\right) D_2 \exp\left[j\left(ct + \frac{ny}{r}\right) - j\frac{nx}{r}\left(\frac{cr}{nU_o} + S_2\right)\right] \qquad (2d)$$

The downstream disturbances are then composed of an irrotational component (the terms proportional to A_2) and vorticity waves which are convected along the mean flow streamlines (the terms proportional to D_2).

The remaining constants (B_1, A_2 and D_2) are determined by the matching conditions across the actuator which relate upstream and downstream flow conditions.

The matching conditions used are

1) Conservation of mass flow
2) Vorticity compatibility (conservation of vorticity)
3) Flow deflection relation

Matching Conditions

The conservation of mass flow through the actuator requires that

$$u_{o_1}(x_{o_1}, y_{o_1}, t_o) = u_{o_2}(x_{o_2}, y_{o_2}, t_o) \qquad (3)$$

where

$$x_{o_1} = 0 \quad ; \quad x_{o_2} = d\cos\delta$$

and

$$y_{o_2} = y_{o_1} + d\sin\delta$$

The vorticity compatibility relation is essentially an application of Helmholtz's law to consider flow with losses.

In vector form, the fluid dynamic equations are

$$\frac{D\vec{V}}{Dt} = \frac{1}{\rho}\nabla p + \vec{f}$$

where

$$\frac{D}{Dt} \equiv \frac{\partial}{\partial t} + V_x\frac{\partial}{\partial x} + V_y\frac{\partial}{\partial y} + V_z\frac{\partial}{\partial z}$$

$$\nabla \equiv i\frac{\partial}{\partial x} + j\frac{\partial}{\partial y} + k\frac{\partial}{\partial z}$$

$$\vec{V} = i\,V_x + j\,V_y + k\,V_z$$

ρ = the density (assumed constant)

p = the static pressure

$\vec{f}$ = the friction force

For a closed circuit C, the circulation is defined as $\Gamma = \oint_C d\vec{r}\cdot\vec{V}$ where $\vec{r}$ is the radius vector to points on C. Then the fluid dynamic equations may be manipulated to obtain

$$\frac{\partial \Gamma}{\partial t} - \oint_c d\vec{r}\cdot(\vec{V}\times\vec{\omega}) = \oint d\vec{r}\cdot\vec{f} \qquad (4)$$

where $\vec{\omega}$ is the vorticity vector.

This equation is strictly applicable to a flow model in which the actual blades are present. For the present type of flow model where the blades are modeled by an actuator, $\vec{f}$ must be modified to include a body force which represents all the forces exerted on the fluid by the blade row. However, only the loss producing or non-conservative forces need to be considered in Eq. (4). The line integral of a conservative force, such as produced by blade lift, around a closed circuit vanishes.

Eq. (4) is the fundamental vorticity compatibility relation. A closed contour, C, is chosen which encloses a portion of the actuator as in Figure 1. Sides (1) and (3) are the boundary of the actuator and sides (2) and (4) are parallel to the blade chords. It is assumed that the unsteady velocity through the actuator is parallel to the blade chords and equal to $u_{o_1}\sec\delta$. It is also assumed that the frictional forces act essentially parallel to the local flow direction such that their contribution to the right hand side of Eq. (4) may be neglected along sides (1) and (3). Use is then made of the following relationship which is derived from integration of the unsteady form of the momentum equation through the actuator.

$$\int_{x_{o_1}}^{x_{o_2}} d\vec{r}\cdot\vec{f} = -\frac{1}{2}\,X\,(\hat{U}_{o_1}^2 + \hat{W}_{o_1}^2)$$

where X is an unsteady total pressure loss coefficient given by

$$X = \frac{H_1 - H_2 - \rho d \sec\delta \frac{\partial u_o}{\partial t_o}}{\frac{1}{2}\rho(\hat{U}_{o_1}^2 + \hat{W}_{o_1}^2)}$$

and H_i is the total pressure relative to the blade row in region i. In general, the unsteady total pressure loss coefficient, X, is different from the steady state loss coefficient. However, in the correlation between theory and experiment which follows in a later section, it was assumed that the unsteady loss coefficient may be approximated by treating the steady state loss coefficient in a quasi-steady fashion.

With the above relation for $\int_{x_{o_1}}^{x_{o_2}} d\vec{r}\cdot\vec{f}$,

the limit of Equation (4) as side ② approaches side ④ is

$$\frac{\partial}{\partial t_o}(\omega_{o_2} - \omega_{o_1}) - d\sec\delta\frac{\partial^2 u_{o_1}}{\partial t_o\,\partial y_o} + U_o(\eta_{o_2} - \eta_{o_1}) = \frac{\partial}{\partial y_o}\left\{\frac{1}{2}X\left[(U_o + u_{o_1})^2 + (W_{o_1} + \omega_{o_1})^2\right]\right\} \quad (5)$$

Here η_o is the z_o component of the vorticity vector and all quantities with a subscript 1 are evaluated at x_{o_1} and y_{o_1} while all quantities with a subscript 2 are evaluated at x_{o_2} and y_{o_2}.

Eq. (5) essentially states that the vorticity shed into the wake is the sum of the time rate of change of the bound vorticity in the actuator plus the vorticity shed due to the loss variation along the actuator axis. Eq. (5) may also be derived in a shorter, but more formal fashion, directly from the equations of motion, and this has been done in Ref. 7, 8, and 9. The present derivation, however, emphasizes concepts and aerodynamic behavior that are familiar from unsteady airfoil theory and results in a closer linkage between rotating stall phenomena and blade row aerodynamics.

The flow deflection relation is obtained from the steady state turning performance of the blade as follows. The steady state turning performance of the cascade is assumed to be expressible in functional notation form as

$$\tan\bar{\beta}_{o_2} = G_{ss}(\tan\bar{\beta}_{o_1})$$

where the subscript ss means steady state. For small unsteady variations in inlet angle about $\bar{\beta}_{o_1}$, the first two terms in the Taylor Series expansion of this equation are used to obtain the quasi-steady relation

$$G_{qs}(\tan\hat{\beta}_{o_1}) \approx G_{ss}(\tan\hat{\beta}_{o_1}) + \sec^2\bar{\beta}_{o_1}\, a\tan\beta'_{o_1}$$

where

$$a = \frac{\partial G_{ss}}{\partial\tan\bar{\beta}_{o_1}} \quad (6)$$

Using the approximation that

$$\tan\hat{\beta}_{o_i} \approx \frac{W_{o_i}}{U_{o_i}} + \frac{\omega_{o_i} - \vartheta_i u_{o_i}}{U_o} \quad (7)$$

the following relation between upstream and downstream swirls may be obtained

$$\omega_{o_2} - \vartheta_2 u_{o_2} = a[\omega_{o_1} - \vartheta_1 u_{o_1}] \quad (8)$$

Eq. (8) is evaluated similarly to Eq. (5). The approximation involved in Eq. (6) is not valid for fully established rotating stall, but it should be valid prior to inception. Eq. (3), (5), and (8) then are the matching conditions between flow conditions upstream and downstream of the blade row. They embody the aerodynamic characteristics attributed to the blade row.

Characteristic Equation

Substitution of the velocity components, Eqs. (2a), (2b), (2c), and (2d) into the matching conditions, Eqs. (3), (5), and (8), yields the following homogeneous system of equations for the unknown constants B_1, A_2, and D_2.

$$\begin{bmatrix} 1 & -e^{\bar{Q}_1} & -e^{\bar{Q}_3} \\ -j\lambda(1+q) - M_1 & -j\lambda e^{\bar{Q}_1} & -[(\lambda+\vartheta_2)\vartheta_2 + 1]e^{\bar{Q}_3} \\ a M_2 & (1 - j\vartheta_2)e^{\bar{Q}_1} & j\lambda e^{\bar{Q}_3} \end{bmatrix} \begin{bmatrix} B_1 \\ A_1 \\ D_2 \end{bmatrix} = 0 \quad (9)$$

where

$$M_1 = (1 + j\vartheta_1)\left[\frac{j}{2}(1+\vartheta_1^2)X' + X\right]$$

$$M_2 = 1 + j\vartheta_1$$

$$\lambda = \frac{cr}{nU_o} + \bar{\Omega}$$

$$q = \frac{dn}{r}\sec\delta$$

$$\bar{Q}_1 = -\frac{nX_{o_2}}{r} + j\frac{dn}{r}\sin\delta$$

$$\bar{Q}_3 = j\left[\frac{dn}{r}\sin\delta - \frac{nX_{o_2}}{r}(\lambda + \vartheta_2)\right]$$

$$X' = \frac{\partial X}{\partial\tan\bar{\beta}_{o_1}}$$

The requirement for a nontrivial solution to Eq. (9) is

$$\begin{bmatrix} 1 & -1 & -1 \\ -j\lambda(1+q) - M_1 & -j\lambda & -[(\lambda+\vartheta_2)\vartheta_2 + 1] \\ a M_2 & (1 - j\vartheta_2) & j\lambda \end{bmatrix} = 0 \quad (10)$$

This is the characteristic equation which determines the allowable values of λ for a nontrivial solution. This equation is a quadratic equation in λ and the first root is found to be the zero amplitude solution previously encountered(11) (12)

$$\lambda_1 = -(\vartheta_2 + j) \quad (11)$$

which has no physical significance. The second root is

$$\lambda = -\frac{1}{2+q}\left\{\frac{1}{2}(1+\vartheta_1^2)X' + \vartheta_1 X + a(\vartheta_1 + \vartheta_2)\right\} \quad (12)$$

$$+ \frac{j}{2+q}\left\{X + 1 + \vartheta_2^2 + a(1 - \vartheta_1\vartheta_2) - \frac{\vartheta_1}{2}(1+\vartheta_1^2)X'\right\}$$

or in terms of C

$$\frac{rC_R}{nU_o} = -\bar{\Omega} - \frac{1}{2+q}\left\{\frac{1}{2}(1+\vartheta_1^2)X' + \vartheta_1 X + a(\vartheta_1 + \vartheta_2)\right\} \quad (13a)$$

$$\frac{rC_I}{nU_o} = \frac{1}{2+q}\left\{X + 1 + \vartheta_2^2 + a(1 - \vartheta_1\vartheta_2) - \frac{\vartheta_1}{2}(1+\vartheta_1^2)X'\right\} \quad (13b)$$

Now $C_I = 0$ implies neutrally stable conditions, $C_I < 0$ implies unstable conditions and $C_I > 0$ implies stable conditions. The propagation velocity of an admissible disturbance is given by

$$V_P = -\frac{r}{n} C_R \qquad (14)$$

The fundamental mechanisms of rotating stall may be identified by analyzing Eq. (13b). First we note that q, X and the product $\mathcal{J}_2 X'$ are positive in regions of interest. Then we see that the only possible destabilizing contributions to C_I come from the last two terms inside the large brackets. The term proportional to a originates in the flow deflection relationship, Eq. (8), and may be either stabilizing or destabilizing. The term proportional to X' originates in the vorticity compatibility relation, Eq. (5), and is always destabilizing. This term may be linked to the vorticity shed into the blade wake by the variation in the time rate of change of losses along the cascade. Without losses and the flow deflection conditions, no instabilities are possible.

From Eq. (13b) the following must be true at the neutral stability points

$$X + 1 + \mathcal{J}_2^2 + a(1 - \mathcal{J}_1 \mathcal{J}_2) - \frac{\mathcal{J}_1}{2}(1 + \mathcal{J}_1^2) X' = 0 \qquad (15)$$

Although the propagation velocity and the damping factor, $\frac{r C_I}{n U_o}$, are in general dependent upon the number of stall cells, Eq. (15) demonstrates that the neutral stability boundary is not.

Correlation With Experiment

The predicted neutral stability boundaries have been compared with the experimentally observed inception boundaries from Ref. 10. This involved comparison with the inception data on five blade rows; four sets were stator rows and one set was a rotor. The tests were performed in the Calspan/Air Force Annular Cascade Facility (which was constructed mainly from the compressor casing of a J-79 jet engine). The hub-to-tip ratio of all the blade rows was 0.8. The blade sets tested were designated as Stator Sets Nos. 1,4,5, and 6 and Rotor Set No. 1. The complete geometric description of these blade sets is given in Ref. 10. Briefly, though, Stator Set No. 1 is a shortened span modification to the original fifth-stage stator row of the J-79 compressor. The blades were 10.6 percent thick at the tip and 8.8 percent thick at the hub. The blades were twisted such that the stagger angle at the hub was 1.42 degrees less than at the tip. It contained 54 blades and the resulting solidity ratio at mid-annulus was 0.85. Stator Set No. 4 had the same airfoil section, twist distribution, and number of blades as Stator Set No. 1 but twice the chord which resulted in twice the solidity. Stator Set No. 5 was Stator Set No. 4 with every other blade removed resulting in the same solidity as Stator Set No. 1. These stator sets had a continuously variable stagger angle. Stator Set No. 6 was a shortened span modification to the original J-79 fifth-stage rotor with 46 blades and a mid-annulus solidity ratio of 0.81. This blade set was tested under rotating and nonrotating conditions. The rotating version of this blade set is desiganted as Rotor Set No. 1. This blade set was only tested at stagger angles of 30°, 40°, and 50°. In all tests, the mean axial flow velocity, U_o, was held constant at 60 feet per second.

The stator sets were tested downstream of a guide vane row which was used to vary the inlet swirl at a fixed stator stagger angle. The inlet swirl was increased until rotating stall was observed on the stator row. Rotor Set No. 1 was tested in isolation at three fixed stagger angles. The rotational speed was varied until rotating stall was incurred. The inception conditions and propagation velocity were measured under all stagger angle conditions tested. Blade row loss and turning performance were measured only at selected stagger angles. The complete set of experimental observations for these blade sets is given in Ref. 10. The inception boundaries for Stator Sets Nos. 1,4, and 5 are summarized in Figs. 2,3, and 4 respectively. The inception boundaries for Stator Set No. 6 and Rotor Set No. 1 are shown in Table 1. For most stagger angles rotating stall first appeared on an intermittent basis and then became steady after a small increase in inlet swirl. (This type of inception is called clean inception). However, for the lower stagger angles on Stator Sets Nos. 1 and 5, the flow became unsteady or turbulent before an identifiable rotating stall was observed, then as the inlet swirl was increased sufficiently a clearly identifiable large amplitude rotating stall was observed.

Table 1 ROTATING STALL INCEPTION BOUNDARY ON STATOR SET NO. 6 AND ROTOR SET NO. 1 AND COMPARISON WITH THEORY

BLADE SET	INCEPTION CONDITIONS				NO OF STALL CELLS (THEORY AND EXP.)
	THEORETICAL		EXPERIMENTAL		
STATOR SET NO. 6	$\mathcal{J}_1$	$Vp/\mathcal{J}_1 Uo$	$\mathcal{J}_1$	$Vp/\mathcal{J}_1 Uo$	
δ_{sm} =30 deg.	-1.90	.20	-1.90*	.40-.50	n = 6
δ_{sm} = 40 deg.	-1.74	.43	-1.67	.46	n = 5
δ_{sm} = 50 deg.	-1.85	.58	-1.74	.42	n = 5
ROTOR SET NO. 1					
δ_{rm} = 30 deg.	-2.23	.2**	-2.18	.76	n = 1
δ_{rm} = 40 deg.	-1.86	.69	-1.86	.61	n = 1
δ_{rm} = 50 deg.	-2.48	.53	-2.51	.47-.53	n = 1

* EXPERIMENT BECOMES TURBULENT AT $\mathcal{J}_1$ = -1.57

** THEORY SHOWS LARGE VARIATION IN Vp NEAR INCEPTION

The theoretical points shown in these comparisons were obtained using the measured blade row performance. The radially averaged turning and loss performance for the blade sets were used to supply the required blade row data for evaluation of Eq. (13a) and (13b). (Generally, the outlet conditions to these blade sets showed strong radial variations of the flow quantities such that radial averaging was required to get a representative picture of the blade row performance). For correlation purposes $\mathcal{J}_1$ was chosen as the independent variable for fixed values of the stagger angles. The experimental values of $\mathcal{J}_2$ and X were spline fit as functions of $\mathcal{J}_1$ for each blade set and stagger angle. These curves were then differentiated to obtain the required values of a and X' as functions of $\mathcal{J}_1$. In this fashion, the damping factor, $\frac{r C_I}{n U_o}$, and propagation velocity were calculated at each inlet swirl to generate a complete stability curve for each case. When the damping factors cross

zero, Eq. (15) is satisfied. Representative stability curves are shown as the dotted lines in Figs. 5 through 8. In each case, the calculations were performed for the number of cells experimentally observed at inception.

In general, the correlation between theory and experiment is good. In most cases in which rotating stall inception is clean the theory predicts the critical inlet swirl within two percent. The swirl is the important parameter from the standpoint of design pressure ratio for a compressor stage. The correlation was limited to the data presented in Ref. 10 because these appear to be the only data available with sufficient information. Although there were guide vanes upstream of the stator sets tested, it will be subsequently shown that these did not affect the inception swirl but only determine the number of stall cells at inception.

Inspection of the stability curves for all the experimental conditions (which are available in Ref. 10) shows that for cases where stall inception was clean, the stability curves behaved as those shown in Figs. 6,7, and 8. That is, there is a relatively sharp decrease in the damping factor in the inception region. For those cases where inception was not clean, the stability curves behaved as shown in Fig. 5. That is, there was a more gradual variation in the damping factor at inception.

Experience with the numerical evaluation of Eq. (13b) and the cascade data has shown that the X' term dominates the a term in controlling the stability of a given flow configuration. From Eq. (13b) it is seen that when

$$X' > \frac{2}{\mathscr{J}_1(1+\mathscr{J}_1^2)}\left\{X + 1 + \mathscr{J}_2^2 + a(1-\mathscr{J}_1\mathscr{J}_2)\right\}$$

an instability results. In the case $a = 0$ (that is when the outlet swirl is independent of the inlet swirl) this result reduces to those obtained in Refs. 7 and 8.

Variation in the Flow Model

The preceding correlations of theory and experiment indicate that the present theory contains at least most of the flow mechanisms that are involved in rotating stall. Hence the present theory should serve as an adequate tool to investigate various features of flow models that have been used in earlier investigations. In particular, a time delay or phase lag in the actuator performance due to the lag time for boundary layer separation has been previously used[1][3]. Also, the analogy of jets discharging into a constant pressure receiver has been proposed by Stenning[3]. (The mathematical statement of this analogy is constant perturbation pressure just downstream of the blade row).

The significance of these two variations in the flow model have been assessed separately by modifying the appropriate portions of the present analysis and solving for the resulting characteristic equation. The downstream constant pressure boundary conditions are considered first.

Constant Pressure Boundary Conditions

In the preceding theory, the requirement that the velocity disturbances be bounded at downstream infinity was imposed as a boundary condition. This is equivalent to imposing a requirement for constant pressure at downstream infinity. In the past, there has been some uncertainty as to the proper downstream boundary condition to impose. The condition of constant pressure just downstream of the blade row was used by Stenning[3] and both conditions were investigated numerically by Takata[9]. However, such questions are not well suited for numerical investigations. Therefore, to explore the question further, the condition of constant pressure just downstream of the blade row was used to replace the bounded velocity requirements at downstream infinity (constant pressure at downstream infinity) in the single blade row analysis. The predictions of the resulting theories are then compared.

The flow configuration shown in Figure 1 and the general form for the disturbance velocities (found from Eq. (1)) apply again. However, in this case $B_2 \neq 0$. It may be shown that the linearized equations of motion admit a solution for the perturbation pressure of the following form

$$P_i = \tilde{P}_i(x)\, e^{j(ct + ny/r)} \qquad (16)$$

in each flow region i. The tangential momentum equation may be used to relate $\tilde{P}_i$ to ϕ_i. The result is

$$\tilde{P}_i = -j\rho U_o \left\{\frac{r}{n}\,\phi_i'' + j\left(\frac{cr}{nU_o} + S_i\right)\phi_i'\right\} \qquad (17)$$

where the primes denote differentiation with respect to x. Then the requirement of constant pressure (no variation with y) just downstream of the actuator becomes

$$\phi_2''(x_{o_2}) + \frac{nj}{r}\left(\frac{cr}{nU_o} + S_2\right)\phi_2'(x_{o_2}) = 0 \qquad (18)$$

where

$$x_{o_2} = d\cos\delta$$

Now Eq. (18) may be combined with Eqs. (3), (5), and (8) to produce the appropriate honogeneous system of equations for the unknowns B_1, A_2, B_2 and D_2. The resulting root of the characteristic equation is

$$\lambda = -\frac{1}{1+q}\left[\frac{1}{2}(1+\mathscr{J}_1^2)X' + \mathscr{J}_1 X + a\mathscr{J}_2\right] \qquad (19)$$
$$+ \frac{j}{1+q}\left[X + 1 + \mathscr{J}_2^2 - a\mathscr{J}_1\mathscr{J}_2 - \frac{\mathscr{J}_1}{2}(1+\mathscr{J}_1^2)X'\right]$$

or in terms of C,

$$\frac{rC_R}{nU_o} = -\bar{\Omega} - \frac{1}{1+q}\left\{\frac{1}{2}(1+\mathscr{J}_1^2)X' + \mathscr{J}_1 X + a\mathscr{J}_2\right\} \qquad (20a)$$

$$\frac{rC_I}{nU_o} = \frac{1}{1+q}\left\{X + 1 + \mathscr{J}_2^2 - a\mathscr{J}_1\mathscr{J}_2 - \frac{\mathscr{J}_1}{2}(1+\mathscr{J}_1^2)X'\right\} \qquad (20b)$$

The neutral stability boundary may be deduced from Eq. (20b) as

$$X + 1 + \mathscr{J}_2^2 - a\mathscr{J}_1\mathscr{J}_2 - \frac{\mathscr{J}_1}{2}(1+\mathscr{J}_1^2)X' = 0 \qquad (21)$$

which is extremely similar to Eq. (15). There are obviously no new mechanisms introduced by use of this boundary condition. Eq. (21) will generally be satisfied at a slightly smaller inlet swirl

than Eq. (15) and the damping factor predicted by Eq. (20b) will generally be larger than those predicted by Eq. (13b). The propagation velocity is more strongly influenced than the inception boundary by the choice of constant pressure boundary conditions. Correlation of Eq. (20a) with data from Rotor Set No. 1 made in Ref. 10 indicate that the propagation velocity is best predicted by using the requirement of constant pressure, or boundedness, at downstream infinity.

Further, if we examine the expression for the downstream pressure perturbation, an anomaly arises. In terms of A_2, B_2, and D_2 Eq. (17) becomes

$$\tilde{P}_2 = -j\rho\frac{nU_o}{r}\left\{A_2\left[1-j(\lambda+\mathcal{S}_2)\right]e^{-nx/r} + B_2\left[1+j(\lambda+\mathcal{S}_2)\right]e^{nx/r}\right\} \qquad (22)$$

First note that the rotational velocity terms (i.e. terms multiplied by D_2) do not contribute to the pressure fluctuations and secondly that even if A_2 and B_2 are selected such that $\tilde{P}_2$ is zero at $x = d\cos\delta$ the pressure is not zero elsewhere in region 2; in fact, it becomes unbounded at downstream infinity. Hence, the boundary condition of bounded disturbances at downstream infinity has been selected in the present work.

Investigation of Time Delay

As mentioned previously, the concept of a time delay for boundary layer separation was thought to be important in the early works on rotating stall. Ref. 1 assumed a phase lag in the actuator characteristics and time delay factors were used in Refs. 3 and 9. The type of time delay used in Refs. 3 and 9 has been investigated in the context of the present theory. This type of time delay was incorporated into the flow deflection relation and the blade row loss characteristic for the single blade row case. The resulting characteristic equation has been obtained and analyzed.

The type of lag time used in Refs. 3 and 9 is incorporated into the blade row turning performance in the following fashion. It is assumed that the unsteady turning performance of the blade row is expressed in functional notation as

$$\tan\hat{\beta}_{o_2} = G(\tan\hat{\beta}_{o_1}) \qquad (23)$$

where G satisfies the relationship

$$\frac{\partial G}{\partial t_o} + \frac{1}{\tau}G = G_{Q.S.} \qquad (24)$$

and where τ is the time delay and G_{QS} is the quasi-steady turning performance of the blade row given by Eq. (6). Then with the use of Eq. (6), Eq. (24) may be integrated to give the blade row response to small sinusoidal inputs in inlet swirl, namely

$$G(\tan\hat{\beta}_{o_1}) = G_{ss}(\tan\bar{\beta}_{o_1}) \qquad (25)$$

$$-\frac{aB_1\frac{n}{rU_o}(1+j\mathcal{S}_1)}{1+j\tau\frac{nU_o}{r}\lambda}\left\{\exp j\left[\lambda\frac{nU_o}{r}t_o+\frac{ny_o}{r}\right]-\exp\left(-\frac{t_o}{\tau}\right)\right\}$$

where G_{ss} is the steady state turning performance of the blade row. Now, although the transient term in Eq. (25) (the second exponential term) will modify the wave shape and change it from a pure sine, it should not affect the long term stability of the system. Hence, it will be discarded in the following analysis.

The loss performance of the blade row is treated similarly. (That is, the same time delay, τ, has been assumed to apply to both the loss and turning relation). Functionally, it is assumed that

$$X = X(\tan\hat{\beta}_{o_1})$$

and that X satisfies a relation similar to Eq. (24). Then the following loss behavior may be deduced

$$X = X_{ss}(\tan\bar{\beta}_{o_1}) \qquad (26)$$

$$-\frac{B_1X'_{ss}\frac{n}{rU_o}(1+j\mathcal{S}_1)}{1+j\tau\frac{nU_o}{r}\lambda}\left\{\exp j\left[\lambda\frac{nU_o}{r}t_o+\frac{ny_o}{r}\right]-\exp\left(-\frac{t_o}{\tau}\right)\right\}$$

where X_{ss} is the steady state loss performance of the blade row and again the transient term will be ignored for stability purposes.

Incorporation of Eq. (25) into the flow deflection matching condition results in

$$\omega_{o_2}(x_{o_2}, y_{o_2}, t_o) - \mathcal{S}_2 u_2(x_{o_2}, y_{o_2}, t_o) = \frac{a}{1+j\bar{\tau}\lambda}\left\{\omega_{o_2}(x_{o_1}, y_{o_1}, t_o) - \mathcal{S}_1 u_{o_1}(x_{o_1}, y_{o_1}, t_o)\right\} \qquad (27)$$

where $\bar{\tau} = \frac{\tau nU_o}{r}$. This replaces Eq. (8) of the previous single blade row analysis. Eq. (26) may be incorporated directly into Eq. (5) to produce the appropriate vorticity compatibility relation for this case. The continuity matching condition remains unchanged for this case and the requirement of bounded flow at upstream and downstream infinity plus the requirement for no vorticity in the incoming flow are used again. Then Eqs. (2), (3), (5), and (27) may be combined to give a homogeneous system for the unknown constants.

After the trivial solution, Eq. (11), has been factored out, the remaining characteristic equation is

$$\bar{A}\lambda^2 + \bar{B}\lambda + \bar{C} = 0 \qquad (28)$$

where

$$\bar{A} = -(2+q)\bar{\tau}$$

$$\bar{B} = j(2+q) + j\bar{\tau}\left[(1+j\mathcal{S}_1)X_{ss} + (1+\mathcal{S}_2^2)\right]$$

$$\bar{C} = (1+j\mathcal{S}_1)\left[X_{ss} + \frac{j}{2}(1+\mathcal{S}_1^2)X'_{ss} + a(1+j\mathcal{S}_2)\right] + (1+\mathcal{S}_2^2)$$

The roots of Eq. (28) are

$$\lambda = \frac{-\bar{B} \pm \sqrt{\bar{B}^2 - 4\bar{A}\bar{C}}}{2\bar{A}} \qquad (29)$$

The mechanisms involved are not readily evident from Eq. (29). However, some interesting proper-

ties of this solution may be obtained by examining the limit as $\bar{\tau} \to 0$.

First, the solution to the previous case without time delay is denoted as λ_o (i.e., the values of λ given by Eq. (12)). Then $\bar{c} = j(2+q)\lambda_o$ and it is seen from Eq. (28) that λ_o is a solution when $\bar{\tau} \to 0$. Furthermore, if either Eq. (28) or (29) is expanded for small $\bar{\tau}$, the following approximate result is obtained, namely

$$\lambda \approx \lambda_o + j \frac{\bar{\tau}\lambda_o}{2+q}\left\{(2+q)\lambda_o + j\left[(1+j\mathscr{A}_1)X_{ss} + (1+\mathscr{A}_2^2)\right]\right\} \tag{30}$$

or in terms of the C,

$$\frac{rC_R}{nU_o} \approx -\bar{\Omega} - \left(\frac{1}{2+q} - \frac{a\bar{\tau}}{(2+q)^2}\right)\left\{\mathscr{A}_1 X_{ss} + \frac{1}{2}(1+\mathscr{A}_1^2)X'_{ss} + a(\mathscr{A}_1 + \mathscr{A}_2)\right\} - \frac{\bar{\tau}}{(2+q)^2}\left[\frac{1}{2}(1+\mathscr{A}_2^2)X'_{ss} - a\mathscr{A}_2\right]\left[1 + \mathscr{A}_2^2 + X_{ss} + a(1-\mathscr{A}_1\mathscr{A}_2) - \frac{1}{2}\mathscr{A}_1(1-\mathscr{A}_1^2)X'_{ss}\right] \tag{31a}$$

$$\frac{rC_I}{nU_o} \approx \left(\frac{1}{2+q} - \frac{a\bar{\tau}}{(2+q)^2}\right)\left\{X + 1 + \mathscr{A}_2^2 - \frac{\mathscr{A}_1}{2}(1+\mathscr{A}_1^2)X'_{ss} + a(1-\mathscr{A}_1\mathscr{A}_2)\right\} - \frac{\bar{\tau}}{(2+q)^2}\left\{\left[\frac{1}{2}(1+\mathscr{A}_1^2)X_{ss} - a\mathscr{A}_2\right]^2 + \left[\frac{1}{2}(1+\mathscr{A}_1^2)X_{ss} - a\mathscr{A}_2\right]\left[\mathscr{A}_1 X_{ss} + a(\mathscr{A}_1 + 2\mathscr{A}_2)\right]\right\} \tag{31b}$$

which are in a form to compare with Eq. (13a) and (13b). Eq. (30) and (31) are well behaved in the limit $\bar{\tau} \to 0$, reducing to the $\bar{\tau} = 0$ case. This is an interesting result since the limiting behavior is not deducible from the fundamental form (e.g., Eq. (24)) in which the time delay was introduced into the analysis.

Recall that $C_I < 0$ corresponds to instability and that $\bar{\tau}$ is always positive. Then, since X_{ss} is positive and generally dominates the terms in the vicinity of the stall boundary, Eq. (31b) would indicate that addition of small time lag to the flow model is usually destabilizing. In fact for lossless flows (i.e., $X_{ss} \equiv 0$) it becomes the primary destabilizing phenomenon. Hence, it was thought to be an important phenomenon in the early investigations[1],[3],[5]. However, the lack of correlation when considering several sets of data[5] plus the good correlation obtained in the present work would indicate that the blade row loss behavior is the important blade row characteristic to model in the theory.

Two Blade Row Theory

The previous analysis considered only a single blade row. In most practical compressors, there are many blade rows closely stacked; hence, it is desirable to develop an applicable theory to handle an arbitrary number of blade rows. The first step of this task, namely a two blade row theory, has been developed and the results will be discussed briefly. The detailed development of the two blade row theory is given in Ref. 10.

The extension of the previous single blade row theory to two blade rows is straightforward but nontrivial. The primary complication that arises is that in this case the characteristic equation is transcendental and must be solved numerically. It has several roots but only one appears to be physically significant, and this root is very close to the single blade row solution. Representative calculations of these roots are shown as the solid curves in Figures 5 through 8. In contrast to the single blade row results, the two blade row stability boundary is dependent upon n, the number of stall cells. Invariably, it was found that there is a minimum value of n below which there were no unstable roots. In general, this value corresponded to the number of stall cells experimentally observed at inception. These values of n are the ones shown in Figs. 5 through 8. The neutral stability boundary for this minimum value of n occurs at a slightly higher absolute value of inlet swirl than that for the single blade row case. At higher values of n the two blade row solution rapidly approaches the single blade row solution. Hence for the cases considered here the single blade row theory predicts the inception condition better, but the two blade row theory indicates that blade row interference controls the number of stall cells that occur at inception.

Concluding Remarks

A stability theory has been developed to predict inception conditions for rotating stall in axial flow compressors. It is shown that if accurate blade row loss and turning performance are known a linearized stability theory is adequate to predict inception. It is shown that the slope of the loss curves versus inlet swirl primarily controls the unsteady vorticity shed into the blade wakes and thereby controls the stability of a given flow configuration. Morevoer, the analysis shows that the inception of rotating stall may be adequately explained in terms of the quasi-steady application of the blade row performance without recourse to a boundary layer lag time or hysteritic blade row performance.

The correlations between theory and experiment indicate that for the high hub-to-tip ratio configurations considered, three dimensional effects per se are not important; they may be accounted for by radially averaging the blade row performance across the annulus.

References

1. Sears, W.R. "Rotating Stall in Axial Compressors" ZAMP, Vol.6, 1955, pp. 429-454.

2. Marble, F.E. "Propagation of Stall in a Compressor Blade Row" JAS, Vol.24, No. 11, November 1957, pp. 541-554.

3. Stenning, A.H., Kriebel, A.R., and Montgomery, S.R., "Stall Propagation in Axial-Flow Compressor" NACA TN 3580, June 1956.

4. Emmons, H.W., Kronauer, R.E., and Rockett, J.A., "A Survey of Stall Propagation--Experiment and Theory", Trans. A.S.M.E. Series D, Vol. 8, September 1959 pp. 409-416.

5. Falk, T.J. "Rotating Stall in Single Stage Axial Flow Compressors" Cornell University, AFOSR TN 56-512 (AD 110327) September 1956.

6. Leone, M.J., "A Study of Existing Information on Rotating Stall With New Observations Concerning Changes in Stall-Cell Size and Number", Rensselaer Polytechnic Inst., TR A.E. 6810 September 1968.

7. Whitehead, D.S. "The Vibration of Cascade Blades Treated by Actuator Disc Methods" A.R.C. Rept. 19 436 EA 594.

8. Rannie, W.D. and Marble, F.E. "Unsteady Flows in Axial Turbomachines" C.R. des Journeles de Sciences Aeronautiques (O.N.E.R.A. France) Part 2, May 1957, pp. 1-21

9. Takata, H. and Nagano, S. "Nonlinear Analysis of Rotating Stall" Trans. A.S.M.E. Series A, Vol. 94, No. 4, pg. 279, October 1972. See also same title, Institute of Space and Aeronautical Science, University of Tokyo, Report No. 449 (1970) April 1970.

10. Ludwig, G.R.; Nenni, J.P. and Arendt, R.H. "Investigation of Rotating Stall in Axial Flow Compressors and the Development of a Prototype Rotating Stall Control System" AFAPL-TR-73-45 May 1973.

11. Brady, W.G. and Ludwig, G.R., Basic Studies of Rotating Stall and an Investigation of Flow-Instability Sensing Devices, Part 1-Basic Studies of Rotating-Stall Flow Mechanisms, AFAPL TR-65-115, Part I, DDC No. AD-625783, October 1965.

12. Ludwig, G.R., Nenni, J.P. and Rice, R.S., Jr., An Investigation of Rotating Stall Phenomena in Turbine Engine Compressors AFAPL-TR-70-26, May 1970.

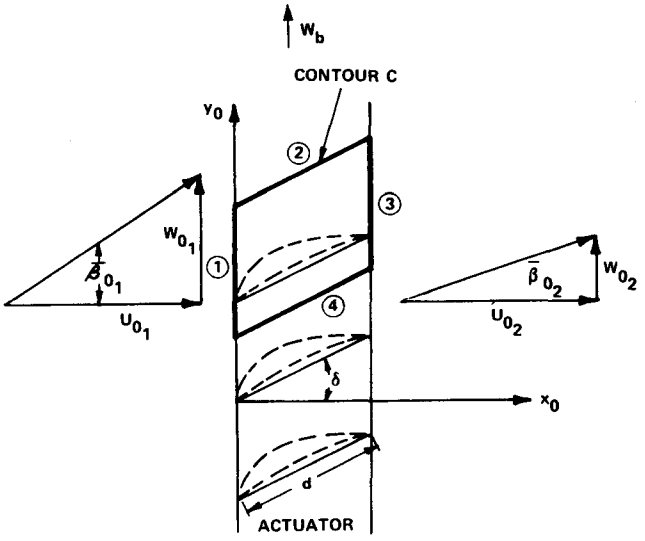

Figure 1 FINITE THICKNESS ACTUATOR MODEL FOR SINGLE BLADE ROW THEORY

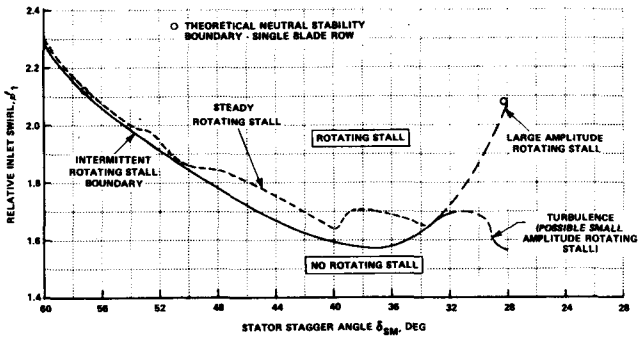

Figure 2 ROTATING STALL INCEPTION BOUNDARY ON STATOR SET NO. 1 AND COMPARISON WITH THEORY

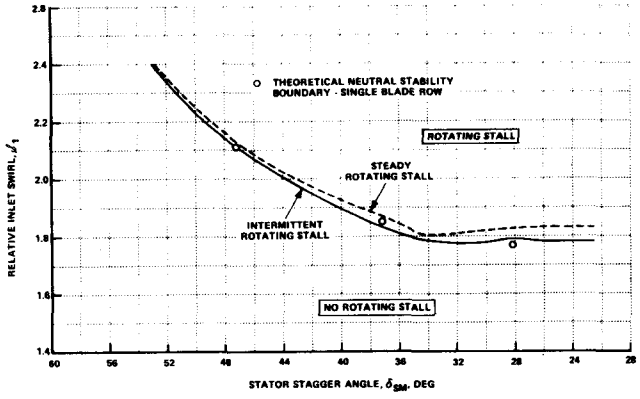

Figure 3 ROTATING STALL INCEPTION BOUNDARY ON STATOR SET NO. 4 AND COMPARISON WITH THEORY

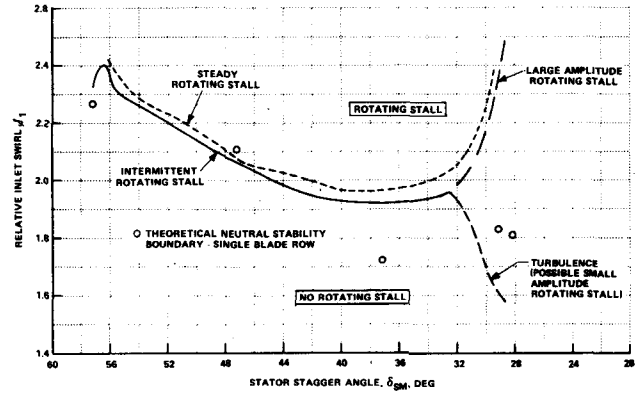

Figure 4 ROTATING STALL INCEPTION BOUNDARY ON STATOR SET NO. 5 AND COMPARISON WITH THEORY

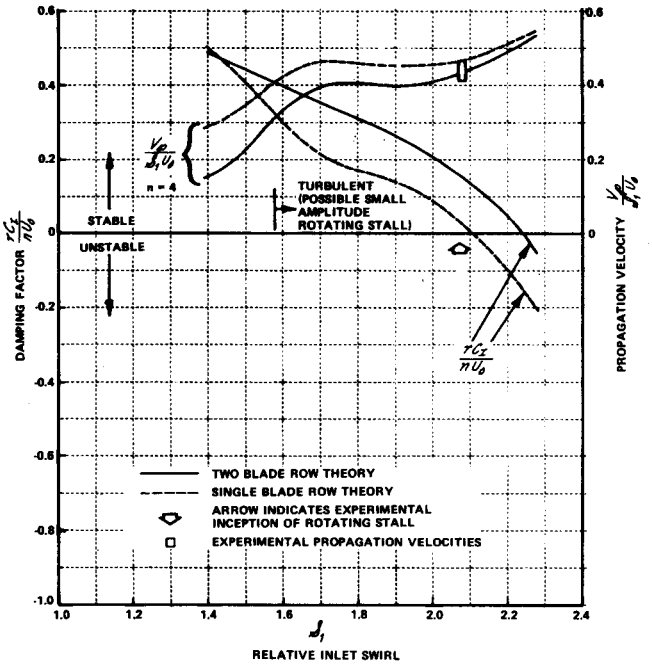

Figure 5 THEORETICAL STABILITY CHARACTERISTICS OF STATOR SET NO. 1

STATOR STAGGER ANGLE, δ_{SM} = 28.2 DEG

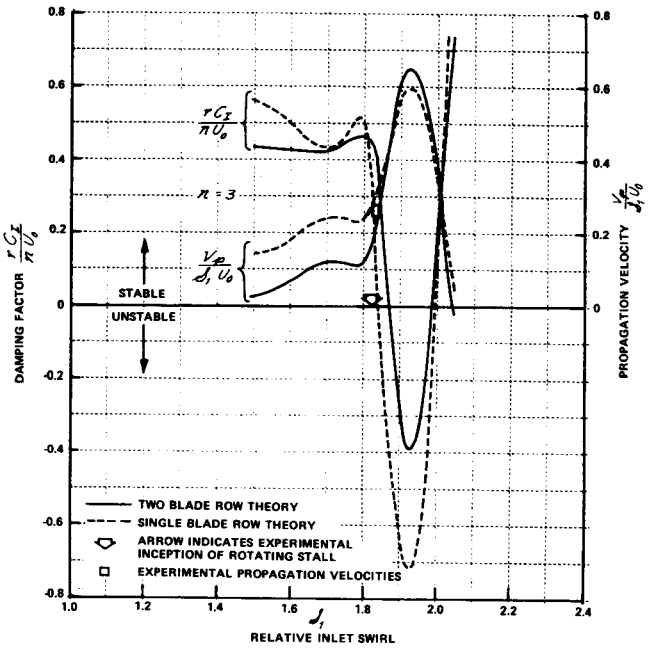

Figure 7 THEORETICAL STABILITY CHARACTERISTICS OF STATOR SET NO. 4

STATOR STAGGER ANGLE, δ_{SM} = 37.2 DEG

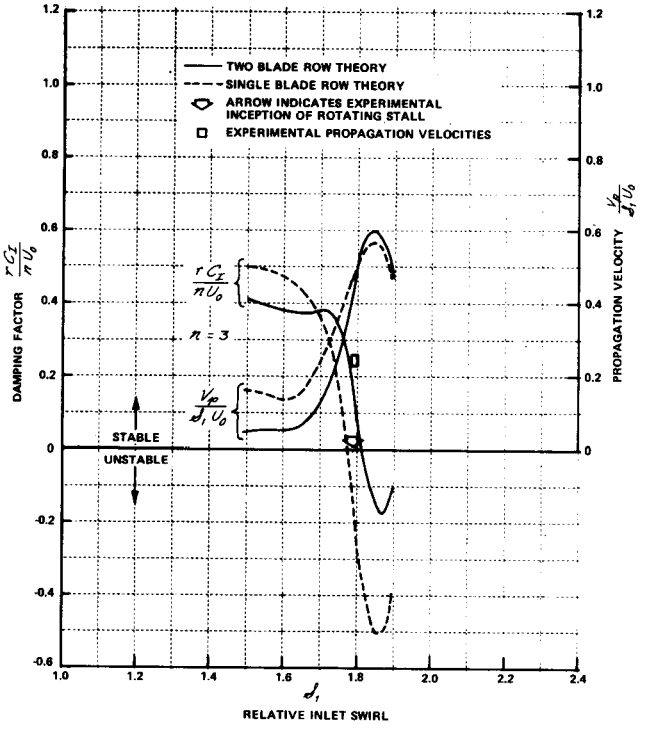

Figure 6 THEORETICAL STABILITY CHARACTERISTICS OF STATOR SET NO. 4

STATOR STAGGER ANGLE, δ_{SM} = 28.2 DEG

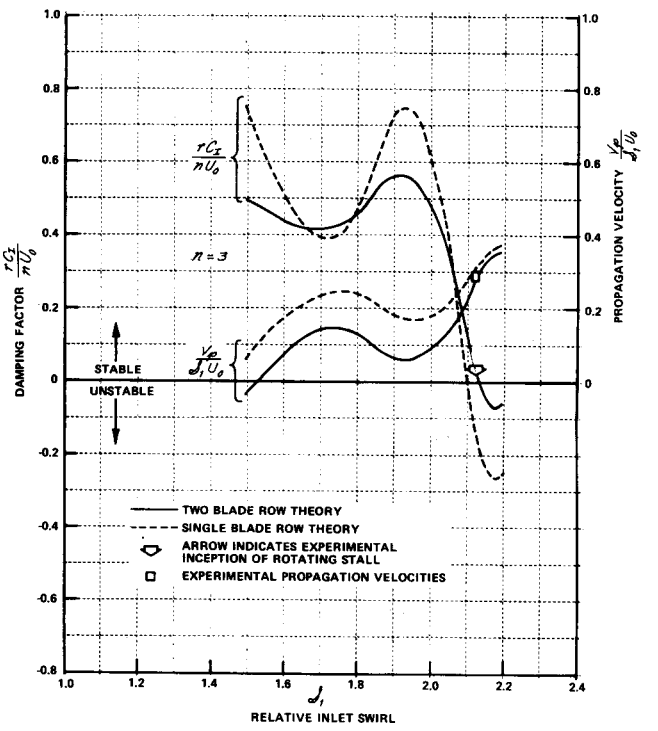

Figure 8 THEORETICAL STABILITY CHARACTERISTICS OF STATOR SET NO. 4

STATOR STAGGER ANGLE, δ_{SM} = 47.2 DEG